

EPS: Efficient Patch Sampling for Video Overfitting in Deep Super-Resolution Model Training

Yiying Wei¹, Hadi Amirpour¹, Jong Hwan Ko², Christian Timmerer¹

¹Christian Doppler Laboratory ATHENA, University of Klagenfurt

²College of Information and Communication Engineering, Sungkyunkwan University

{yiying.wei, hadi.amirpour, christian.timmerer}@aau.at, jhko@skku.edu

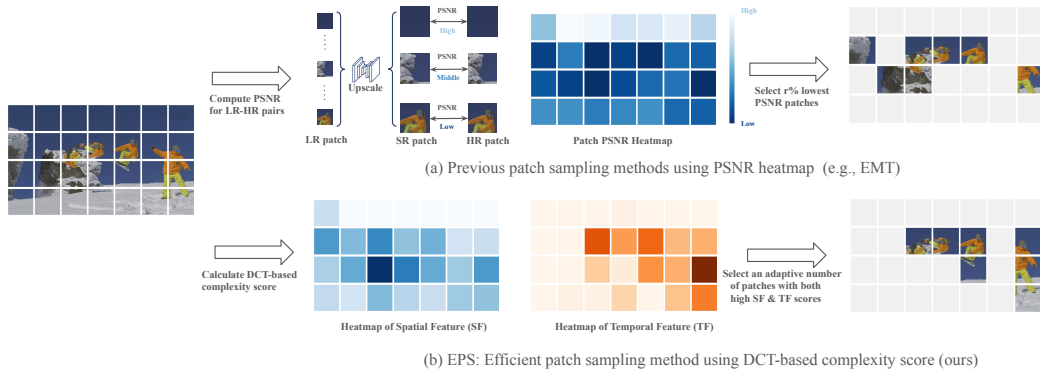


Figure 1. (a) State-of-the-art patch sampling methods compute PSNR for each LR-HR patch pair to extract the informative patches. (b) **EPS**: Efficient patch sampling directly uses DCT-based complexity scores (*SF* and *TF*) to select informative patches. The *SF* score indicates the complexity of the texture information within the patch itself, while the *TF* score indicates movement and change between frames to help reduce temporal redundancies for patch sampling.

Abstract

Leveraging the overfitting property of deep neural networks (DNNs) is trending in video delivery systems to enhance quality within bandwidth limits. Existing approaches transmit overfitted super-resolution (SR) model streams for low-resolution (LR) bitstreams, which are used to reconstruct high-resolution (HR) videos at the decoder. Although these approaches show promising results, the huge computational costs of training a large number of video frames limit their practical applications. To overcome this challenge, we propose an efficient patch sampling method named **EPS** for video SR network overfitting, which identifies the most valuable training patches from video frames. To this end, we first present two low-complexity Discrete Cosine Transform (DCT)-based spatial-temporal features to measure the complexity score of each patch directly. By analyzing the histogram distribution of these features, we then categorize all possible patches into different clusters and select training patches from the cluster with the highest spatial-temporal information. The number of sampled

patches is adaptive based on the video content, addressing the trade-off between training complexity and efficiency. Our method reduces the number of patches for the training to 4% to 25%, depending on the resolution and number of clusters, while maintaining high video quality and significantly enhancing training efficiency. Compared to the state-of-the-art patch sampling method, EMT, our approach achieves an 83% decrease in overall run time.

1. Introduction

With the ever-increasing amount of video content, video applications, and the ongoing evolution of video in various dimensions, such as spatial resolution and temporal resolution (frame rate), transmitting high-quality, high-resolution videos presents a significant challenge. In response to these challenges, new video codecs have been introduced, such as Versatile Video Coding (VVC) [6] or AOMedia Video 1 (AV1) [8], which employ more efficient compression techniques to help transmit high-quality video content while reducing bandwidth requirements. However, these video cod-

ing methods still face limitations to further improve compression performance, as they rely on hand-crafted techniques and highly engineered modules.

With the development of deep learning, leveraging deep neural networks (DNNs) to enhance video compression has become a new trend in modern video transmission systems. Numerous learning-based video compression methods [7, 19, 20, 29] have been proposed to deliver high-quality video streams to users. Among these approaches, an emerging number of approaches integrate super-resolution (SR) techniques to reduce bandwidth requirements [10, 11, 23]. These methods transmit low-bitrate low-resolution (LR) videos and super-resolve them to high-resolution (HR) videos on the end-user device by applying pre-trained SR models. These SR models are typically trained on a limited dataset and may encounter difficulties adapting to new video content. However, creating a universal DNN model that excels with all Internet videos is impractical. To overcome this limitation, recent advances in neural-enhanced video delivery [5, 12, 13, 18, 31] leverage the overfitting property of DNNs to achieve quality improvements. These approaches train an SR model for **each video** and stream the LR video along with the corresponding content-aware SR model to the end-user device. The reinforced expressive power of content-aware SR models significantly improves the quality of resolution-upscaled videos.

Although neural-enhanced video delivery shows promising performance, the huge computational cost of training content-aware SR models limits its practical applications. With a linear increase in the input video resolution, the approach cannot be easily adapted to live streaming with stringent delay requirements. Additionally, it is essential to acknowledge that deploying such models for large-scale video processing and delivery workflows entails significant energy consumption, which poses challenges in terms of sustainability and environmental impact [1].

To reduce the computational cost of network training, EMT [17] proposed a patch sampling method to select the most informative patches using a *patch PSNR heatmap*, showing training gains comparable to using all frames. Specifically, it uses (i) a pre-trained SR model to super-resolve all LR patches of one frame, and then (ii) calculates their PSNR values with the original HR patches to generate the patch PSNR heatmap. As shown in Fig. 1(a), the patch PSNR heatmap varies across different patch locations according to its content. Regions with complex textures usually represent lower PSNR values than smooth regions because they are more challenging to restore with an SR model. The patch PSNR heatmap indeed partially reflects the texture complexity of patches, assisting in the identification of valuable patches for training content-aware models. However, the current state-of-the-art patch sampling methods, such as [17], still have two main drawbacks:

- First, generating patch PSNR heatmaps for all frames is time-consuming. It requires additional computational resources, as it involves the inference of a DNN and calculating PSNR for each patch, which online training attempts to avoid.
- Second, these methods sample patches only based on the SR quality comparisons without considering the temporal redundancy between frames. When temporal complexity is low – indicating that a patch is similar to its co-located patch in the previous frame – it can be excluded from the training set due to the redundancy, thus reducing unnecessary computational load.

In this paper, we propose Efficient Patch Sampling (EPS) for high-quality and efficient video super-resolution. As illustrated in Fig. 1(b), our method leverages spatial-temporal information to quickly select the most informative patches from video frames without the need to super-resolve frames and calculate the quality. We introduce two DCT-based features to directly evaluate the spatial and temporal complexity of patches in LR video frames. Compared to PSNR heatmaps that rely on DNN inference and are calculated on patches after SR by comparing them to the corresponding HR patches, DCT is a low-complexity computation on LR patches that enables faster execution on both CPU and GPU, significantly speeding up informative patch scoring. Instead of simply selecting the complex patches of each frame, we sample the patches by considering both temporal and spatial dimensions as the training set for the content-aware SR model. Our approach excludes relatively static patches across frames from repeated training, thereby reducing temporal redundancies.

Our contributions can be summarized as follows.

- We introduce two low-complexity DCT-based informative features to measure the spatial-temporal complexity of each LR-HR patch pair. This approach is fast and effective in guiding the selection of the most informative patches, making the content-aware training gain appear as large and quickly as possible (*cf.* Sec. 3.1).
- We present a novel patch sampling algorithm for content-aware video SR training, which utilizes histogram distribution of patch features for clustering to select the patches with the highest spatial-temporal information. By considering temporal information, our method effectively removes redundant patches across consecutive frames, further enhancing training efficiency. The number of sampled patches is adaptive based on the content and addresses the trade-off between training cost and efficiency (*cf.* Sec. 3.2).
- We conduct comprehensive experiments based on various SR architectures to evaluate the advantages and generalization of our method (*cf.* Sec. 4).

2. Related Work

Content-aware Neural Video Delivery. NAS [31] was among the first proposed neural-enhanced video delivery frameworks to integrate a per-video SR model. A DNN is trained for each LR video content, and both the LR video and its associated DNN are delivered to the client side, which are jointly used to enhance its quality. LiveNAS [13] proposed a live video ingest framework that integrates an online training module into the original NAS approach [31]. However, content-aware SR models with large parameters still introduce an overhead to the delivery process. SRVC [12] encodes a video into content streams and time-varying model streams, updating only a fraction of the model parameters over video chunks to handle the available bandwidth budget better. DeepStream [5] utilizes compressed content-aware SR networks to achieve significant bitrate savings while maintaining the same quality for end-user devices with GPU capabilities. Nevertheless, these approaches still demand significant computational resources for training the network; however, utilizing patch sampling can mitigate this requirement.

Patch Sampling. In the online training module of LiveNAS [13], they sample fixed-size LR-HR patches from **random** locations in a given frame. However, employing a random sampling method may lead to selecting suboptimal patches for training. In practice, more complex patches in texture may contribute significantly to model training [13, 26, 33]. EMT [17] used the PSNR of the HR patch and the decoded LR patch upscaled by the SR model, demonstrating higher precision in identifying complex patches that yield greater training gains. However, evaluating an SR model on all possible patch pairs is time-consuming and brings additional costs. Furthermore, these methods do not fully exploit the spatial information of a single frame, particularly **temporal information between frames**. Ignoring spatial-temporal information can result in suboptimal and redundant training data, thereby reducing the training efficiency. Our work differs from these works by sampling complex patches using simple yet efficient DCT-based features that account for both spatial and temporal information. We note that some efficient SR methods [15, 16, 28] also leverage the patch complexity. However, these methods aim to accelerate execution speed by training all patches with SR models at multiple scales to handle various patch complexities. Therefore, we do not compare our patch sampling method with these works, as data sampling can further accelerate them.

3. Efficient Patch Sampling (EPS)

In this section, we present our efficient patch sampling method to accelerate the training with reduced computational costs. Fig. 2 shows an overview of our proposed

method. We first split the LR video into frames and divide each frame into a grid of non-overlapping patches. Our method leverages both spatial and temporal features to evaluate the texture complexity of each patch. We then group all patches into N clusters according to the histogram distribution of our proposed features. The patches of the cluster with the **highest** spatial-temporal information are selected to train a content-aware SR model. We first introduce the features to evaluate the patch complexity in both spatial and temporal dimensions in Sec. 3.1. We then propose a patch sampling algorithm to determine the most valuable training patches for the SR model training in Sec. 3.2.

3.1. Patch Features

Related work [13, 17] shows that more informative patches provide higher training gains than others. Given that not all parts of the video are equally important for training, patch sampling aims to quickly select challenging patches and discard uninformative or redundant patches. To efficiently sample patches that achieve the goal, we introduce two informative features for each patch: (i) Spatial Feature (SF) and (ii) Temporal Feature (TF).

The complexity of a patch is related to its frequency components, where a higher proportion of high frequencies typically indicates a more complex texture and content. Thus, we assess the informative features of patches based on their frequency components. Following the work in [14, 21] that groups image pixels into regions of similar textures using the *Discrete Cosine Transform* (DCT), we use a DCT-based energy function to map the texture of a patch from a multiple-dimensional frequency space into a one-dimensional energy space. This energy function reflects the spatial complexity of the patch, which is denoted as SF . The SF of a patch is defined as:

$$SF = \sum_{i=0}^{w-1} \sum_{j=0}^{h-1} e^{[(\frac{ij}{wh})^2 - 1]} |DCT(i, j)| \quad (1)$$

where w and h are the width and height of the patch, and $DCT(i, j)$ is the $(i, j)^{th}$ DCT component when $i + j > 0$, and 0 otherwise. The SF function assigns exponentially higher costs to higher DCT frequencies since we expect the highest frequencies to be caused by a mixture of objects.

TF defines the complexity of the temporal variation between video frames and is computed as the difference of the DCT component of each patch of the current frame compared to its previous frame. Formally, we denote the total T frames of the given LR video as I_1, I_2, \dots, I_T . For a patch of frame I_t ($1 < t \leq T$), the TF is defined as follows:

$$TF_t = \sum_{i=0}^{w-1} \sum_{j=0}^{h-1} e^{[(\frac{ij}{wh})^2 - 1]} |DCT(i, j)_t - DCT(i, j)_{t-1}| \quad (2)$$

Example heatmaps of SF and TF are shown in Fig. 3 ($w = 64, h = 64$). A high SF score represents complex texture and rich patch information. Consequently, a

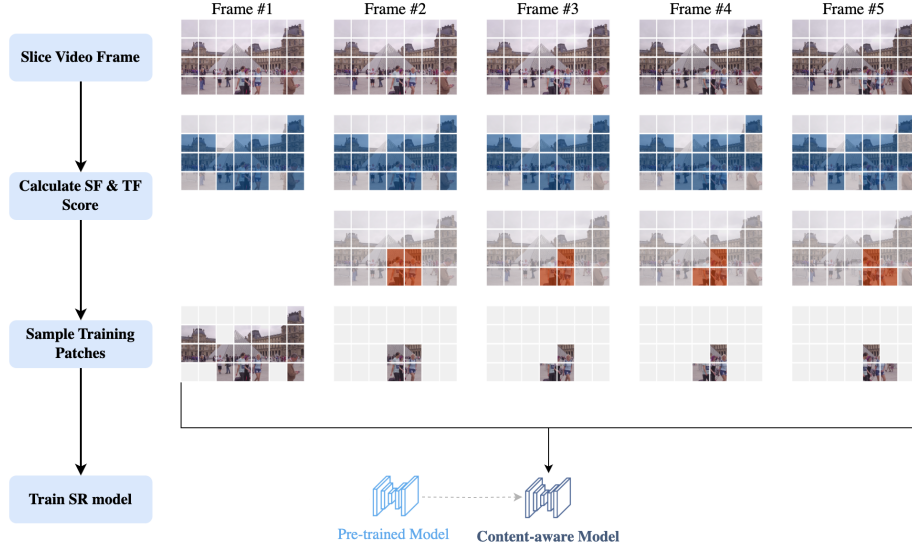


Figure 2. The overview of EPS method. Each video frame is sliced into patches. The informative complexity of each patch is determined by spatial features (SF) and temporal features (TF). For each frame, we group all patches into N clusters based on the histogram distribution of feature scores and select the cluster of **highest** spatial-temporal information for training a content-aware SR model (using a pre-trained model as a basis). In the figure, we set the number of clusters to two for better readability. The blue and orange patches represent clusters with high SF and TF scores, respectively.

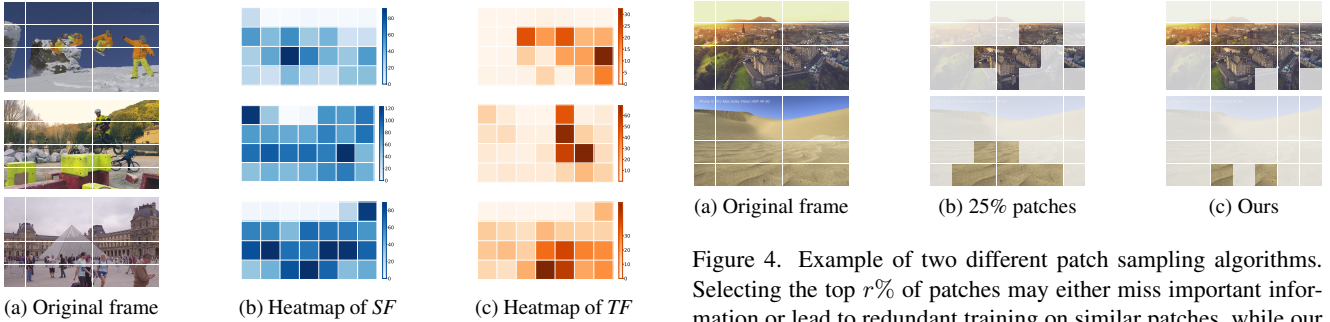


Figure 3. Example heatmaps of SF and TF scores of the video frames from the Inter4K dataset [25].

high TF score indicates that the patch in frame I_t has obvious changes compared to I_{t-1} . Therefore, the TF serves as an indicator of redundancy in co-located patches across frames.

3.2. Patch Sampling Algorithm

In this section, we propose a spatial-temporal patch sampling algorithm. Previous works [13, 17] have relied on setting fixed thresholds for sampling simply by selecting the top $r\%$ of patches according to their information complexity. However, such sampling methods do not take into account the varied distribution of patch information

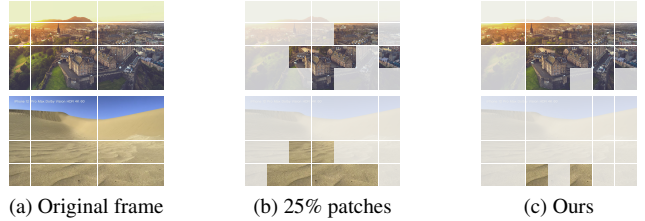


Figure 4. Example of two different patch sampling algorithms. Selecting the top $r\%$ of patches may either miss important information or lead to redundant training on similar patches, while our sampling algorithm mitigates these issues.

complexity across different video contents. For individual videos, this direct sampling approach may overlook important information or overly train on simpler information. As shown in Fig. 4, in a complex video, sampling 25% of patches might still exclude informative patches, whereas, in a simple video, the same percentage could include non-informative content. Therefore, we utilize the histogram distribution of spatial-temporal features for clustering to conduct patch sampling. Algorithm 1 shows our patch sampling algorithm, which selects patches with the highest spatial-temporal information and discards uninformative or redundant patches. The goal is to sample LR-HR patch pairs P to train a content-aware SR model of a T -

Algorithm 1 Patch Sampling Strategy

Input: Video frame sequences $\{I_1, I_2, \dots, I_t, \dots, I_T\}$, Number of clusters N

Output: Sampled training patches P

```
1: for  $t = 1 \rightarrow T$  do
2:    $m = \text{sliceFrame}(I_t)$  // Slice frame  $I_t$  to  $m$  patches
3:    $SF = \text{calcSF}(m)$  // Calculate  $SF$  scores for  $m$  patches according to Eq. (1)
4:    $C_{SF} = \text{cluster}(m, N, SF)$  // Group  $m$  into  $N$  clusters based on  $SF$ , i.e. the  $N$  bins of  $SF$  histogram
5:    $C_{SF} = \text{rank}(C_{SF})$  // Rank  $SF$  clusters from low to high  $\{C_{SF_1}, \dots, C_{SF_N}\}$ 
6:   if  $t > 1$  then
7:      $TF = \text{calcTF}(m)$  // Calculate  $TF$  scores for  $m$  patches according to Eq. (2)
8:      $C_{TF} = \text{cluster}(m, N, TF)$  // Group  $m$  into  $N$  clusters based on  $TF$ , i.e. the  $N$  bins of  $TF$  histogram
9:      $C_{TF} = \text{rank}(C_{TF})$  // Rank  $TF$  clusters from low to high  $\{C_{TF_1}, \dots, C_{TF_N}\}$ 
10:  end if
11:  if  $t == 1$  then
12:     $P_1 = C_{SF_N}$ 
13:  else
14:     $P_t = C_{SF_N} \cap C_{TF_N}$ 
15:  end if
16: end for
17: return  $P = \{P_1, P_2, \dots, P_t, \dots, P_T\}$ 
```

frame video sequence.

Suppose that the resolution of a given LR video is $W \times H$, and the LR patch size is $w \times h$. The corresponding HR patch width and height are $w \times k$ and $h \times k$, where k is the scaling factor. As shown in Fig. 3, we slice a frame into patches of C columns and L rows. Therefore, the total number of patches for each frame is $C \times L$. Note that the $C = \lfloor \frac{W}{w} \rfloor$ and the $L = \lfloor \frac{H}{h} \rfloor$ are integer numbers, ignoring the possible remaining borders of the frame.

For the first frame I_1 , we obtain the SF scores for all patches according to Eq. (1), and then list these SF values as a monotonically increasing histogram. Based on the distribution of this histogram, we partition all these patches into N clusters, corresponding to the N bins of the histogram. This means that the distribution of patch numbers among different clusters is based on information density. The training set P_1 is defined as the patches from the highest SF cluster C_{SF_N} , which are expected to possess the most informative and challenging texture characteristics.

For all subsequent frames I_t ($2 \leq t \leq T$), we sample informative patches considering both spatial and temporal complexity. The SF and TF of all patches in I_t are calculated in parallel using Eq. (1) and Eq. (2), respectively. These SF and TF scores are individually listed as two histograms, and the corresponding patches are partitioned into N -numbered SF clusters and N -numbered TF clusters (C_{SF} , C_{TF}). We take patches in the highest SF and TF clusters as the training set P_t . Note that in some cases, P_t might be an empty set, which means that no training patches are meeting the requirements for this frame, thereby

reducing the total number of patches. Finally, all the selected patches from each frame are combined as the final training set P . This approach saves time and computational resources and maintains model performance when no new information is available for fine-tuning.

Fig. 5 shows an example of the proposed patch sampling algorithm for the second frame of video #0048 from the Inter4K dataset [25]. We adjust the number of sampled patches by grouping the SF and TF scores into N clusters, which are based on the number of bins in the histogram.

4. Experiments

In this section, we describe our experiments to evaluate the performance of our proposed method. Sec. 4.1 comprises information about the video dataset used for our experiments and implementation details. In Sec. 4.2, we compare our approach EPS with various neural video delivery methods, including both non-sampling methods and recent patch sampling methods. Finally, in Sec. 4.3, we present our ablation study on key parameters demonstrating the impact on (i) cluster number N , (ii) training epoch, (iii) patch size, (iv) and quantization parameter.

4.1. Experimental Settings

We aim to assess our method across various content complexities, thus selecting a dataset comprising diverse scenes, motions, and objects. For this study, we adopted the first 100 video sequences from the Inter4K dataset [25]. We apply bicubic downsampling to downscale the original version to a resolution of 1920×1080 to be used as *HR video*. For *LR video*, we utilize two scaling factors, i.e., $\times 2$ and $\times 4$, and all LR videos are compressed with four quantization parameters (QPs) values, i.e., $\{22, 27, 32, 37\}$ using the x265 encoder¹. The set of videos with QP 27 is utilized as the default dataset. Peak Signal-to-Noise Ratio (PSNR) and Video Multi-Assessment Method Fusion (VMAF) [22] are adopted as evaluation metrics to measure SR performance. All PSNR and VMAF values are the average values of 100 videos. To verify the effectiveness and generalization of our method, we conduct the experiments using four SR architectures, including FSRCNN [9], ESPCN [24], CARN [4], and WDSR [32]. We selected these SR models for their real-time potential and compatibility with related works. All experiments were conducted with the PyTorch framework on NVIDIA RTX 6000 Ada GPUs. The LR patch size is set to 64×64 during training unless mentioned otherwise. We use Adam optimizer with $\beta_1 = 0.9$, $\beta_2 = 0.999$, $\epsilon = 10^{-8}$ and we use L1 loss as loss function. The mini-batch size is 64, and the learning rate is 10^{-4} . All models are trained 300 epochs from a pre-trained model using the

¹<https://x265.readthedocs.io/en/master/index.html>, last access: November 10, 2024.

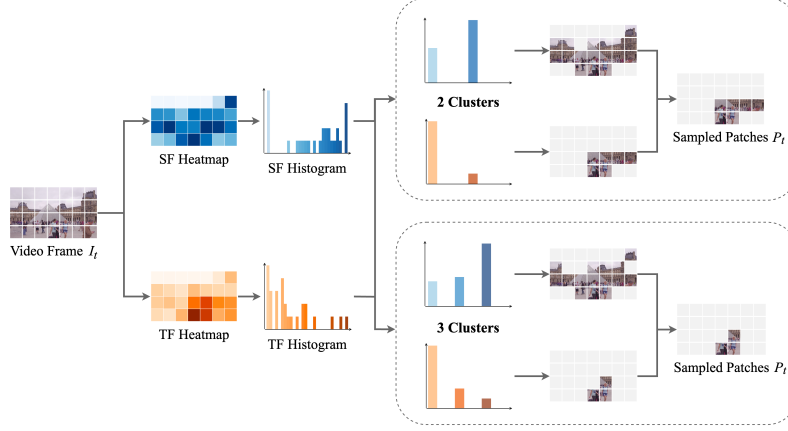


Figure 5. Example of the proposed patch sampling algorithm for $N = \{2, 3\}$.

above experimental setups. Pre-trained models are trained using the DIV2K [2] and Flickr2K [3] datasets without any compression, but they lack training data from the Inter4K [25] dataset, making them suitable for our content-aware training.

We compare our method with other neural video delivery methods, including agDNN [30] where a video is super-resolved by a content-agnostic DNN (*i.e.*, a pre-trained model without overfitting), NAS [31] that fine-tunes the pre-trained model to fit all patches of the video without patch sampling, LiveNAS [13] that randomly samples patches to train the content-aware model, and EMT [17] that calculates the patch PSNR heatmap to select the $r\%$ most challenging patches of each frame to train the SR model. To assess the overfitting quality, we train content-aware SR models using the same pre-trained SR model. In the EPS method, the histogram distributions of SF and TF differ across video contents, leading to variations in the number of patches used for training. Here, we set the number of clusters to two in EPS and calculate the average number of training patches used across all videos. For different patch sampling methods, all training parameters and the number of training patches are kept constant, with the only difference being the selected patches.

For training with only small subsets of data, there are some similar approaches, such as dataset distillation [27] and active learning [34]. However, these methods are not applicable to the content-aware SR model training task in this paper. First, we aim to select a small portion of data for model overfitting on video content, so it is important to preserve the original data details. Fine-tuning the model based on a synthesized dataset may not adequately address the overfitting problem and could result in suboptimal performance. Therefore, we do not compare with dataset distillation. Secondly, utilizing a deep neural network for patch selection is costly for our task. Such network training would result in additional time requirements and increased com-

putational overhead. Identifying and labeling the impact of each patch on the model’s performance is also expensive. Given a p -frame video with q patches per frame, $2^{(p \times q)}$ training sessions are required to obtain labels. To mitigate these expenses, we only consider training-free approaches.

4.2. Comparison with Related Works

Tab. 1 shows a comprehensive quantitative comparison with various SR models under different scaling factors. As can be seen, EPS consistently achieves similar or even higher quality performance² compared to the NAS trained with all available patches. EPS also demonstrates improved performance over other patch sampling methods (*i.e.*, LiveNAS and EMT) using the same number of patches. The qualitative comparison is shown in Fig. 6.

For the $\times 2$ scaling factor, the LR video has a resolution of 960×540 . We partition each 30-frame video sequence into a total of 3,600 patches, which equals 120 patches per frame. Through our patch sampling algorithm in Sec. 3.2, we select an average of 21 out of 120 patches per frame (*i.e.*, 17.5%) for content-aware training, resulting in similar or even slightly better training gains compared to NAS. This might be because training NAS over non-informative patches reduces the model’s overall effectiveness. In the case of the $\times 4$ scaling factor, the LR video has a resolution of 480×270 , resulting in 840 patches for a 30-frame video sequence. The overall patch count is reduced from 840 to an average of 225 (*i.e.*, 26.78%), using the proposed patch selection algorithm. The quality achieved by the content-aware DNN, measured by PSNR and VMAF, is significantly superior to the content-agnostic DNN (agDNN) for NAS and EPS. In some cases, there is even an improvement in EPS compared to NAS, which uses all patches for training. Conversely, models with larger parameter sizes, like CARN and WDSR, exhibit a moderate decrease in quality

²Best performing methods are marked bold for all backbone SR architectures; overall winners are in blue.

Table 1. Comparison of SR results between content-agnostic DNN method (agDNN [30]), content-aware method using all patches for training (NAS [31]), and content-aware approach using different patch sampling approach LiveNAS [13], EMT [17] and EPS (ours). Results are averaged across all frames over all sequences².

Scale Factor	Method	Patches	FSRCNN		ESPCN		CARN		WDSR	
			PSNR	VMAF	PSNR	VMAF	PSNR	VMAF	PSNR	VMAF
$\times 2$	agDNN [30]	0 %	26.15	79.72	32.40	82.12	35.41	88.90	35.83	89.49
	NAS [31]	100.00 %	34.74	84.61	33.96	83.46	36.12	89.14	36.72	90.10
	LiveNAS [13]	17.50 %	33.60	80.01	33.27	83.14	35.76	88.95	36.27	89.47
	EMT [17]	17.50 %	34.26	85.13	34.49	84.52	35.89	89.03	36.71	90.02
	EPS (ours)	17.50 %	34.85	85.71	34.61	85.08	36.42	89.91	36.78	90.19
$\times 4$	agDNN [30]	0 %	24.15	47.95	29.44	43.01	30.86	64.09	30.69	63.92
	NAS [31]	100.00 %	29.99	51.75	29.90	50.77	31.89	69.71	31.87	69.66
	LiveNAS [13]	26.78 %	29.27	48.37	29.65	47.75	30.93	64.67	31.20	67.53
	EMT [17]	26.78 %	30.09	52.71	29.86	51.35	31.21	68.34	31.48	69.07
	EPS (ours)	26.78 %	30.16	54.17	30.06	52.14	31.77	69.25	31.79	69.55

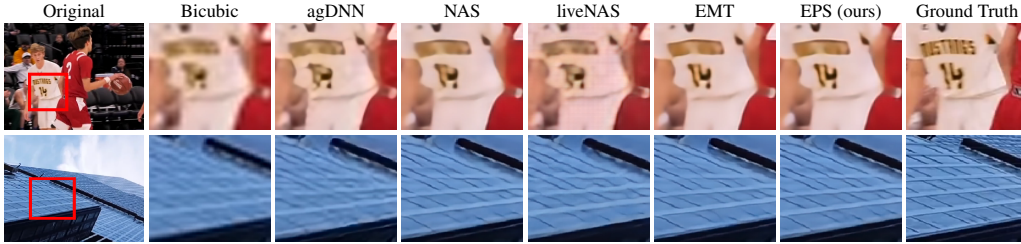


Figure 6. Super-resolution quality comparison using our method (seventh column) with baseline methods.

Table 2. Impact of cluster number. The Patches column denotes the average portion of patches utilized for training².

Scale Factor	#Clusters	Patches	FSRCNN		ESPCN		CARN		WDSR	
			PSNR	VMAF	PSNR	VMAF	PSNR	VMAF	PSNR	VMAF
$\times 2$	1	100.00 %	34.74	84.61	33.96	83.46	36.12	89.14	36.72	90.10
	2	17.50 %	34.85	85.68	34.50	84.51	36.42	89.91	36.78	90.19
	3	8.04 %	34.79	85.71	34.49	84.74	36.06	89.55	36.48	89.92
	4	4.72 %	34.73	85.58	34.54	84.87	35.86	89.31	36.27	89.64
	5	3.26 %	34.56	85.43	34.37	84.59	35.58	89.17	36.12	89.48
$\times 4$	1	100.00 %	29.99	51.75	29.90	50.77	31.89	69.71	31.87	69.66
	2	26.78 %	30.16	54.17	30.06	52.14	31.67	69.25	31.79	69.55
	3	14.42 %	30.13	54.49	30.04	52.37	31.28	68.51	31.62	69.44
	4	9.70 %	30.11	54.62	30.07	52.71	31.19	67.67	31.43	68.94
	5	7.23 %	30.04	54.64	30.06	52.89	30.98	67.05	31.26	68.45

at the $\times 4$ scale. However, EPS can highly reduce the training data of the model with only a negligible drop in quality compared to NAS.

LiveNAS has a fast sampling speed due to the random selection of patches, but the training gain is significantly lower than that of EPS trained with all patches. While our approach demonstrates better performance compared to EMT, it is equally crucial to assess the time required during patch selections. We measured the average execution time for sampling the same number of LR-HR patches from 100 videos. It was observed that our approach achieves an 83% decrease in overall run time compared to EMT. The disparity in run time is linked to the parallel-friendliness of our approach, where the computations of SF and TF can be performed concurrently. In general, our EPS method for the same number of selected patches achieves higher quality at a significantly reduced run time.

4.3. Ablation Study

▷ **Impact of Cluster Number.** We conduct extensive experiments to explore the content-aware SR performance under different numbers of clusters during patch sampling, which is shown in Tab. 2. For an SR model with a very small size of parameters like FSRCNN and ESPCN, even a limited patch selection can yield promising results. However, for CARN and WDSR, as the number of clusters separated by histogram bins increases, indicating a minimal portion of the selected patches, the trained SR model exhibits a slight quality drop, specially in the case of $\times 4$ scale.

▷ **Impact of Training Epoch.** We intend to explore how adjusting the training epochs affects the performance of SR models, given that content-aware training takes advantage of the overfitting property of DNNs. We train all models from pre-trained initialization to 300 epochs in scaling factor $\times 4$ for every 100 epochs across all videos, using differ-

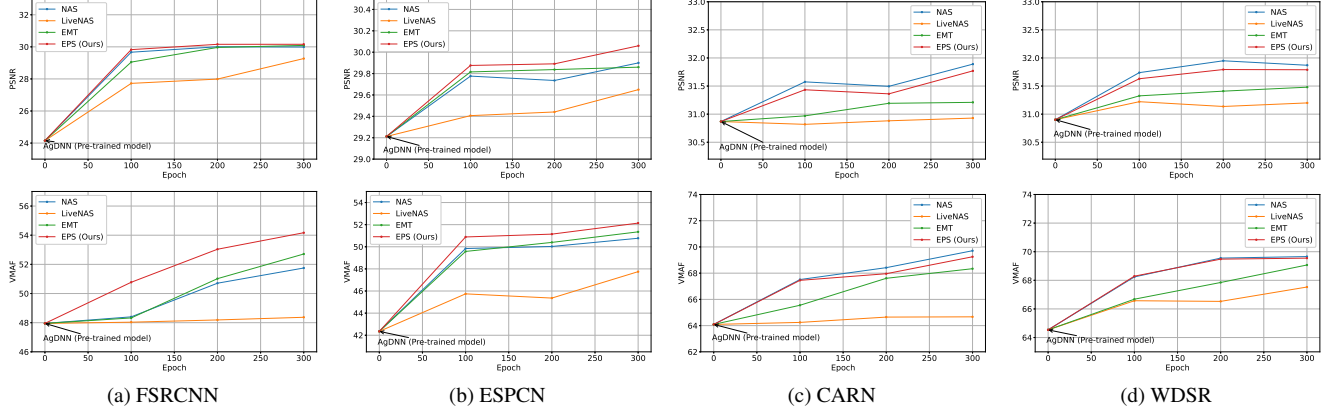


Figure 7. Comparison of video quality for all models ($\times 4$) between content-aware models when all patches are selected for training (NAS) and when different sampling approaches are utilized (LiveNAS, EMT, and EPS) for every 100 epochs.

ent patch sampling methods. As can be seen in Fig. 7, compared to NAS that training with all patches, models trained with our sampled patches achieve better SR video quality with similar or much lower training epochs. It indicates that when all patches are selected for training, the model undergoes fine-tuning for both informative and non-informative patches, leading to lower performance compared to when only informative patches are utilized for training. Compared to other patch sampling methods like LiveNAS and EMT, our EPS method gets significantly higher training gains using the same number of sampled patches. This indicates that EPS is more effective at selecting informative patches, allowing the content-aware SR model to learn from higher-quality data.

▷ **Impact of Patch Size.** During the experiments, we slice each LR frame into patches of 64×64 by default. We also study the effect of different patch sizes. We evaluated all models using the sampling method through a two-cluster histogram and calculated their training gains based on the pre-trained initialization. The result for each patch size is reported as the average training gains of four models. As shown in Tab. 3, all patch sizes achieve similar results with negligible quality differences, showcasing that our sampling method is suitable for various patch sizes.

Table 3. Variants of patch size.

Patch Size	$\times 2$		$\times 4$	
	Δ PSNR	Δ VMAF	Δ PSNR	Δ VMAF
64×64	+3.21	+2.66	+2.15	+6.54
32×32	+3.18	+2.72	+2.20	+6.65
16×16	+3.20	+2.69	+2.12	+6.58

▷ **Impact of Quantization Parameter.** To investigate the impact of input LR video qualities on the training effectiveness of the SR model, we conduct experiments to handle the compressed video datasets with $QP = \{22, 27, 32, 37\}$. For each QP, we train all models to evaluate their SR performance

Table 4. Variants of Quantization Parameter (QP).

QP	$\times 2$		$\times 4$	
	Δ PSNR	Δ VMAF	Δ PSNR	Δ VMAF
22	+3.30	+2.79	+2.23	+6.71
27	+3.21	+2.66	+2.15	+6.54
32	+3.17	+2.51	+2.08	+6.39
37	+3.01	+2.02	+1.94	+6.05

and report the average training gain compared to the pre-trained model. The results in Tab. 4 show that as the QP increases, the quality of the SR video gradually decreases since the LR video introduces more distortion. However, our method can still achieve promising training improvement at high QP (*i.e.*, $QP=37$).

5. Conclusion

In this paper, we propose an efficient patch sampling method for leveraging the overfitting property of DNNs in content-aware training for video SR models. To reduce the computational costs while maintaining the overfitting quality, we sample the most informative patches from video frames to accelerate training. To achieve this, we initially partition frames into non-overlapping patches and assess texture and motion complexity using two DCT-based metrics: SF (spatial feature) and TF (temporal feature). Subsequently, for each frame, we group SF and TF values into N clusters and select patches belonging to the N^{th} cluster in both SF and TF . Our approach achieves comparable or even superior SR quality performance compared to models trained with all data, thus significantly reducing the training input. Our approach undergoes extensive experimentation across diverse video content involving 100 video sequences. We assess its effectiveness and generalizability by employing four SR architectures: FSRCNN, ESPCN, CARN, and WDSR. Our patch sampling approach is observed to reduce the number of patches to 4% to 25% of the original

dataset, depending on the resolution and the input number of clusters (N). Compared to the state-of-the-art, it selects more informative patches for training while consuming a significantly lower computational cost. Furthermore, our approach demonstrates efficiency in various ablation studies, varying the number of clusters, training epochs, patch sizes, and quantization parameters.

References

- [1] Samira Afzal, Narges Mehran, Zoha Azimi Ourimi, Farzad Tashtarian, Hadi Amirpour, Radu Prodan, and Christian Timmerer. A Survey on Energy Consumption and Environmental Impact of Video Streaming. 2024. Publisher: arXiv Version Number: 1. [2](#)
- [2] Eirikur Agustsson and Radu Timofte. Ntire 2017 challenge on single image super-resolution: Dataset and study. In *The IEEE Conference on Computer Vision and Pattern Recognition (CVPR) Workshops*, July 2017. [6](#)
- [3] Eirikur Agustsson and Radu Timofte. Ntire 2017 challenge on single image super-resolution: Dataset and study. In *2017 IEEE Conference on Computer Vision and Pattern Recognition Workshops (CVPRW)*, pages 1122–1131, 2017. [6](#)
- [4] Namhyuk Ahn, Byungkong Kang, and Kyung-Ah Sohn. Fast, accurate, and lightweight super-resolution with cascading residual network. In *Computer Vision – ECCV 2018: 15th European Conference, Munich, Germany, September 8-14, 2018, Proceedings, Part X*, page 256–272, Berlin, Heidelberg, 2018. Springer-Verlag. [5](#)
- [5] Hadi Amirpour, Mohammad Ghanbari, and Christian Timmerer. DeepStream: Video Streaming Enhancements using Compressed Deep Neural Networks. *IEEE Transactions on Circuits and Systems for Video Technology*, pages 1–1, 2022. [2, 3](#)
- [6] Benjamin Bross, Ye-Kui Wang, Yan Ye, Shan Liu, Jianle Chen, Gary J. Sullivan, and Jens-Rainer Ohm. Overview of the Versatile Video Coding (VVC) Standard and its Applications. *IEEE Transactions on Circuits and Systems for Video Technology*, 31(10):3736–3764, Oct. 2021. [1](#)
- [7] Tong Chen, Haojie Liu, Qiu Shen, Tao Yue, Xun Cao, and Zhan Ma. Deepcoder: A deep neural network based video compression. In *2017 IEEE Visual Communications and Image Processing (VCIP)*, pages 1–4, 2017. [2](#)
- [8] Yue Chen, Debargha Mukherjee, Jingning Han, Adrian Grange, Yaowu Xu, Sarah Parker, Cheng Chen, Hui Su, Urvang Joshi, Ching-Han Chiang, and et al. An overview of coding tools in av1: the first video codec from the alliance for open media. *APSIPA Transactions on Signal and Information Processing*, 9:e6, 2020. [1](#)
- [9] Chao Dong, Chen Change Loy, and Xiaoou Tang. Accelerating the super-resolution convolutional neural network. In Bastian Leibe, Jiri Matas, Nicu Sebe, and Max Welling, editors, *Computer Vision – ECCV 2016*, pages 391–407, Cham, 2016. Springer International Publishing. [5](#)
- [10] A. Dosovitskiy, P. Fischer, E. Ilg, P. Hausser, C. Hazirbas, V. Golkov, P. Smagt, D. Cremers, and T. Brox. FlowNet: Learning optical flow with convolutional networks. In *2015 IEEE International Conference on Computer Vision (ICCV)*, pages 2758–2766, Los Alamitos, CA, USA, dec 2015. IEEE Computer Society. [2](#)
- [11] A. Habibi, T. Rozendaal, J. Tomczak, and T. Cohen. Video compression with rate-distortion autoencoders. In *2019 IEEE/CVF International Conference on Computer Vision (ICCV)*, pages 7032–7041, Los Alamitos, CA, USA, nov 2019. IEEE Computer Society. [2](#)
- [12] M. Khani, V. Sivaraman, and M. Alizadeh. Efficient video compression via content-adaptive super-resolution. In *2021 IEEE/CVF International Conference on Computer Vision (ICCV)*, pages 4501–4510, Los Alamitos, CA, USA, oct 2021. IEEE Computer Society. [2, 3](#)
- [13] Jaehong Kim, Youngmok Jung, Hyunho Yeo, Juncheol Ye, and Dongsu Han. Neural-enhanced live streaming: Improving live video ingest via online learning. In *Proceedings of the Annual conference of the ACM Special Interest Group on Data Communication on the applications, technologies, architectures, and protocols for computer communication*, pages 107–125, 2020. [2, 3, 4, 6, 7](#)
- [14] Michael King, Zinovi Tauber, and Ze-Nian Li. A new energy function for segmentation and compression. In *2007 IEEE International Conference on Multimedia and Expo*, pages 1647–1650, 2007. [3](#)
- [15] Xiangtao Kong, Hengyuan Zhao, Yu Qiao, and Chao Dong. ClassSR: A general framework to accelerate super-resolution networks by data characteristic. In *Proceedings of the IEEE/CVF conference on computer vision and pattern recognition*, pages 12016–12025, 2021. [3](#)
- [16] G. Li, J. Ji, M. Qin, W. Niu, B. Ren, F. Afghah, L. Guo, and X. Ma. Towards high-quality and efficient video super-resolution via spatial-temporal data overfitting. In *2023 IEEE/CVF Conference on Computer Vision and Pattern Recognition (CVPR)*, pages 10259–10269, Los Alamitos, CA, USA, jun 2023. IEEE Computer Society. [3](#)
- [17] Xiaoqi Li, Jiaming Liu, Shizun Wang, Cheng Lyu, Ming Lu, Yurong Chen, Anbang Yao, Yandong Guo, and Shanghang Zhang. Efficient meta-tuning for content-aware neural video delivery. In *Computer Vision – ECCV 2022: 17th European Conference, Tel Aviv, Israel, October 23–27, 2022, Proceedings, Part XVIII*, page 308–324, Berlin, Heidelberg, 2022. Springer-Verlag. [2, 3, 4, 6, 7](#)
- [18] Jiaming Liu, Ming Lu, Kaixin Chen, Xiaoqi Li, Shizun Wang, Zhaoqing Wang, Enhua Wu, Yurong Chen, Chuang Zhang, and Ming Wu. Overfitting the data: Compact neural video delivery via content-aware feature modulation. In *Proceedings of the IEEE/CVF International Conference on Computer Vision*, pages 4631–4640, 2021. [2](#)
- [19] Guo Lu, Chunlei Cai, Xiaoyun Zhang, Li Chen, Wanli Ouyang, Dong Xu, and Zhiyong Gao. Content adaptive and error propagation aware deep video compression. In *Computer Vision–ECCV 2020: 16th European Conference, Glasgow, UK, August 23–28, 2020, Proceedings, Part II 16*, pages 456–472. Springer, 2020. [2](#)
- [20] Guo Lu, Wanli Ouyang, Dong Xu, Xiaoyun Zhang, Chunlei Cai, and Zhiyong Gao. Dvc: An end-to-end deep video compression framework. In *Proceedings of the IEEE/CVF Conference on Computer Vision and Pattern Recognition*, pages 11006–11015, 2019. [2](#)

- [21] Vignesh V Menon, Christian Feldmann, Hadi Amirpour, Mohammad Ghanbari, and Christian Timmerer. VCA: Video Complexity Analyzer. In *Proceedings of the 13th ACM Multimedia Systems Conference*, pages 259–264, June 2022. 3
- [22] Reza Rassool. Vmaf reproducibility: Validating a perceptual practical video quality metric. In *2017 IEEE International Symposium on Broadband Multimedia Systems and Broadcasting (BMSB)*, pages 1–2, 2017. 5
- [23] Oren Rippel, Sanjay Nair, Carissa Lew, Steve Branson, Alexander G Anderson, and Lubomir Bourdev. Learned video compression. In *Proceedings of the IEEE/CVF International Conference on Computer Vision*, pages 3454–3463, 2019. 2
- [24] W. Shi, J. Caballero, F. Huszar, J. Totz, A. P. Aitken, R. Bishop, D. Rueckert, and Z. Wang. Real-time single image and video super-resolution using an efficient sub-pixel convolutional neural network. In *2016 IEEE Conference on Computer Vision and Pattern Recognition (CVPR)*, pages 1874–1883, Los Alamitos, CA, USA, jun 2016. IEEE Computer Society. 5
- [25] Alexandros Stergiou and Ronald Poppe. Adapool: Exponential adaptive pooling for information-retaining downsampling. *IEEE Transactions on Image Processing*, 32:251–266, 2023. 4, 5, 6
- [26] Mariya Toneva, Alessandro Sordoni, Remi Tachet des Combes, Adam Trischler, Yoshua Bengio, and Geoffrey J Gordon. An empirical study of example forgetting during deep neural network learning. *arXiv preprint arXiv:1812.05159*, 2018. 3
- [27] Tongzhou Wang, Jun-Yan Zhu, Antonio Torralba, and Alexei A Efros. Dataset distillation. *arXiv preprint arXiv:1811.10959*, 2018. 6
- [28] Yan Wang, Yi Liu, Shijie Zhao, Junlin Li, and Li Zhang. CAMixerSR: Only Details Need More” Attention”. In *Proceedings of the IEEE/CVF Conference on Computer Vision and Pattern Recognition*, pages 25837–25846, 2024. 3
- [29] Chao-Yuan Wu, Nayan Singhal, and Philipp Krähenbühl. Video compression through image interpolation. In *ECCV*, 2018. 2
- [30] Hyunho Yeo, Sunghyun Do, and Dongsu Han. How will deep learning change internet video delivery? In *Proceedings of the 16th ACM Workshop on Hot Topics in Networks, HotNets ’17*, page 57–64, New York, NY, USA, 2017. Association for Computing Machinery. 6, 7
- [31] Hyunho Yeo, Youngmok Jung, Jaehong Kim, Jinwoo Shin, and Dongsu Han. Neural adaptive content-aware internet video delivery. In *13th USENIX Symposium on Operating Systems Design and Implementation (OSDI 18)*, pages 645–661, 2018. 2, 3, 6, 7
- [32] Jiahui Yu, Yuchen Fan, Jianchao Yang, Ning Xu, Xinchao Wang, and Thomas S Huang. Wide activation for efficient and accurate image super-resolution. *arXiv preprint arXiv:1808.08718*, 2018. 5
- [33] Geng Yuan, Xiaolong Ma, Wei Niu, Zhengang Li, Zhenglun Kong, Ning Liu, Yifan Gong, Zheng Zhan, Chaoyang He, Qing Jin, et al. Mest: Accurate and fast memory-economic sparse training framework on the edge. *Advances in Neural Information Processing Systems*, 34:20838–20850, 2021. 3
- [34] Jifan Zhang, Julian Katz-Samuels, and Robert Nowak. Galaxy: Graph-based active learning at the extreme. In *International Conference on Machine Learning*, pages 26223–26238. PMLR, 2022. 6